Acta Materialia 188 (2020) 486–491

Contents lists available at ScienceDirect

Acta Materialia

journal homepage: www.elsevier.com/locate/actamat

Full length article

Vanadium is an optimal element for strengthening in both fcc and bcc high-entropy alloys

Binglun Yin[a,*], Francesco Maresca[a,b], W.A. Curtin[a]

[a] Laboratory for Multiscale Mechanics Modeling (LAMMM) and National Centre for Computational Design and Discovery of Novel Materials (NCCR MARVEL), École Polytechnique Fédérale de Lausanne, Lausanne 1015, Switzerland
[b] Faculty of Science and Engineering, Engineering and Technology Institute Groningen, University of Groningen, 9747 AG, The Netherlands

ARTICLE INFO

Article History:
Received 27 October 2019
Revised 14 January 2020
Accepted 29 January 2020
Available online 6 February 2020

Keywords:
High-entropy alloys
Vanadium
Solute strengthening theory
Yield strength

ABSTRACT

The element Vanadium (V) appears unique among alloying elements for providing high strengthening in both the fcc Co-Cr-Fe-Mn-Ni-V and bcc Cr-Mo-Nb-Ta-V-W-Hf-Ti-Zr high-entropy alloy families. The origin of Vanadium's special role is its atomic volume: large in the fcc alloys and small in the bcc alloys, and thus having a large misfit volume in both crystalline structures. A parameter-free theory applicable to both fcc and bcc HEAs rationalizes this finding, with predictions of strength across a range of fcc and bcc alloys in quantitative and qualitative agreement with experiments. In the fcc class, the analysis demonstrates why the newly-discovered NiCoV and $Ni_{0.632}V_{0.368}$ alloys have far higher strength than any other fcc alloy and are predicted to be the highest attainable. In the bcc class, the analysis demonstrates that the addition of V always increases the strength relative to the same alloys without V. The optimization of complex alloys for high strength should thus center around the inclusion of V as a primary element at concentration levels of around 25 at.%

1. Introduction

High-entropy alloys (HEAs) are multicomponent alloys with high concentrations of all alloying elements. Alloys within this new class of structural metal alloys demonstrate impressive combinations of properties such as high strength and high fracture toughness [1–4]. These attractive properties have driven an intense search for new alloys across the full range of number of components and composition. Designing new alloys or rationalizing alloy performance has, however, frequently relied on imprecise and non-quantitative concepts or correlations, such as "lattice distortions" [5–8], electronegativity differences [9] and others [10]. With a vast composition space available for alloy design, physically-based and quantitatively-predictive theories are needed to guide the search for better-performing alloys while understanding the limits of performance. In fact, such theories have recently been developed for predicting alloy yield strength [11,12] and have been shown to predict experiments across a range of HEA systems. The success of these theories indicates that the solute misfit volumes are the dominant factor in strengthening. This insight points toward new promising alloy compositions in different alloy classes [12–14]. Theoretical results to date are on only a narrow range of alloys, and no fcc alloys containing Vanadium (V) have been studied. However, experimentally, alloys containing the element V provide the highest strengthening in both fcc and bcc alloys.

The primary experimental evidence for the role of V is revealed by examining two alloy families. In the fcc family of Co-Cr-Fe-Mn-Ni-V, the medium-entropy alloy NiCoV [5] and the binary alloy $Ni_{0.632}V_{0.368}$ [9] have recently been reported to have very high room temperature strengths as compared to all other alloys in this family. In the bcc refractory alloy family Mo-Nb-Ta-V-W, the MoNbTaVW has the highest retained strength at very high temperatures ($T > 1500$ K) [15,16]. The fundamental origins of these extreme properties and their connections to the alloy composition were not previously established nor was the role of V as the critical element in both fcc and bcc recognized. Here, application of the new mechanistic models [11,12] for strengthening in fcc and bcc HEAs explains the origin of V's potency for strengthening in HEAs. In particular, we make new quantitative predictions for the NiCoV and $Ni_{0.632}V_{0.368}$ fcc alloys in good agreement with experiments. These findings point toward future development of V-containing alloys as most promising for creating high strengths in both fcc and bcc alloys.

High strength is not the sole requirement in alloy design. The high strength may compromise ductility, for instance. For V, the low melting point of Vanadium oxide may limit the application of V-containing alloys to non-oxidizing situations. However, these issues may also be overcome by tuning of other alloying elements or by engineering mitigation strategies such as protective coatings, enabling the exploitation of the high strength provided by V-containing alloys.

* Corresponding author.
E-mail address: binglun.yin@epfl.ch (B. Yin).

https://doi.org/10.1016/j.actamat.2020.01.062
1359-6454/

2. Solute strengthening theory

The theoretical framework for understanding the special role of V is based on the fundamental interaction energy between a dislocation and the solutes that constitute the random alloy. In the random alloy, the random arrangement of solutes gives rise to spatially-fluctuating total interaction energies between the dislocation and the collective fluctuations in local solute concentrations. The dislocation becomes pinned in regions of favorable fluctuations, and this pinning is associated with high barriers for dislocation motion. These barriers are overcome only by high applied stresses and/or high temperatures. A new general theory for the strength of random alloys based on the motion of edge dislocations through the random alloy, and encompassing both fcc and bcc crystal structures and for arbitrary number of components and arbitrary composition, embodies the physics of the problem [11,12]. The full theory for the finite-T, finite-strain-rate initial yield strength of an alloy can be reduced to an approximate analytical model under the assumption that the solute/dislocation interaction energy U^n of a type-n solute is governed by elasticity theory, i.e., $U^n = -p\Delta V_n$, where ΔV_n is the misfit volume of the type-n solute ($n = 1, \ldots, N$) in a N-component alloy and p is the pressure field generated by the dislocation at the solute position. The theory then predicts the zero-temperature shear yield stress τ_{y0} and the energy barrier ΔE_b for thermally activated flow as

$$\begin{aligned}\tau_{y0} &= A_\tau \alpha^{\frac{1}{3}} \mu_{\text{alloy}} \left[\frac{1+\nu_{\text{alloy}}}{1-\nu_{\text{alloy}}}\right]^{\frac{4}{3}} \left[\frac{\sum_n c_n \Delta V_n^2}{b^6}\right]^{\frac{2}{3}}, \\ \Delta E_b &= A_E \alpha^{\frac{1}{3}} \mu_{\text{alloy}} b^3 \left[\frac{1+\nu_{\text{alloy}}}{1-\nu_{\text{alloy}}}\right]^{\frac{2}{3}} \left[\frac{\sum_n c_n \Delta V_n^2}{b^6}\right]^{\frac{1}{3}}.\end{aligned} \tag{1}$$

At finite temperature T and finite strain rate $\dot{\epsilon}$, standard thermal activation theory then leads to the predicted tensile yield stress as

$$\sigma_y(T, \dot{\epsilon}) = 3.06\tau_{y0}\left[1 - \left(\frac{kT}{\Delta E_b}\ln\frac{\dot{\epsilon}_0}{\dot{\epsilon}}\right)^{\frac{2}{3}}\right]. \tag{2}$$

Here, $\dot{\epsilon}_0 = 10^4$ s^{-1} is a reference strain rate and 3.06 is the Taylor factor for isotropic fcc and bcc polycrystals strengths controlled by edge dislocations. The quantities μ_{alloy} and ν_{alloy} are the shear modulus and Poisson's ratio of the alloy and $\alpha = 0.125$ (fcc) or 0.0833 (bcc) is related to the edge dislocation line tension as $\Gamma = \alpha\mu_{\text{alloy}}b^2$. For fcc elastically anisotropic materials, the best estimates for μ_{alloy} and ν_{alloy} are the Voigt averages [17], with the shear modulus in the line tension expression the value for the glide plane/direction of the dislocations. Often, however, only the isotropic polycrystalline moduli are available from experiments which leads to some underestimate of the strength.

The prefactor coefficients (A_τ,A_E) emerge from the reduced elasticity theory that depends only on the solute misfit volumes and the dislocation pressure field. These two material properties emerge as separated in the theory. The pressure field then depends only on the alloy elastic constants and dislocation core structure (distribution of Burgers vector), and so the coefficients (A_τ,A_E) depend only on these properties. Calculations [11,12] of the typical atomistic structures of the (dissociated) fcc edge dislocation and the (undissociated) bcc edge dislocation lead to accurate alloy-independent prefactors $(A_\tau, A_E) = (0.01785, 1.5618)$ for fcc alloys and $(A_\tau, A_E) = (0.040, 2.00)$ for bcc alloys, reflecting the different atomic structures of fcc and bcc edge dislocations. The details of full and reduced theory can be found in Ref. [11] for fcc alloys and Ref. [12] for bcc alloys.

The theory demonstrates that the solute misfit volumes control strengthening because the alloy elastic moduli vary more slowly with composition. The misfit volumes ΔV_n of each type-n element ($n = 1, \ldots, N$) in N-component random alloys at composition $\{c_n\}$ can be calculated as

$$\Delta V_n = \frac{\partial V_{\text{alloy}}}{\partial c_n} - \sum_{m=1}^{N} c_m \frac{\partial V_{\text{alloy}}}{\partial c_m}, \tag{3}$$

with alloy atomic volume $V_{\text{alloy}} = V_{\text{alloy}}(c_1, c_2, \ldots, c_{N-1})$ and $\partial V_{\text{alloy}}/\partial c_N = 0$ [18]. Therefore, the misfit volumes can be (i) measured experimentally [18], (ii) sometimes computed accurately by first-principles methods [14], or (iii) estimated. A widely-used approximation is Vegard's law $V_{\text{alloy}} = \sum_n c_n V_n$, leading to misfit volumes $\Delta V_n = V_n - V_{\text{alloy}}$ where V_n is the apparent volume of type-n element in the given crystal structure.

It is important to note several misconceptions related to the determination of misfit volumes that have arisen specifically in the study of V-containing alloys of interest here. First, the apparent volume of a solute is not the local Voronoi-volume around the solute in the lattice. The misfit volume involves distortions that extend to near-neighbor atoms and beyond, and the formal definition above (Eq. 3) encompasses all possible situations without the need to identify local atomic-scale details. Second, the misfit volume of a solute must be calculated in the alloy itself, or in an appropriate surrogate alloy having the same solute concentration. A misfit volume computed in a surrogate alloy in the dilute solute limit may be quite inaccurate because Vegard's law does not always hold with sufficient accuracy. Below, we will show the errors caused by these estimates of misfit volume in the case of V.

With this broad background, we can now proceed to understand why the unique role of V for strengthening in both fcc and bcc HEAs is due to its atomic volume.

3. Results

3.1. Application of theory to fcc HEAs

We first consider the fcc Co-Cr-Fe-Mn-Ni-V family of HEAs, i.e., adding V to the well-established Cantor alloy family. We have computed the atomic volume of fcc V as 13.914 Å^3 using first-principles spin-polarized DFT as implemented in VASP [19], where PBE [20] is used as the exchange-correlation functional and the PAW [21] pseudopotential includes V (3s, 3p, 4s, 3d) as the valence states. (Detailed DFT parameters can be found in Ref. [14].) As shown in Table 1, this atomic volume is far larger than the apparent atomic volumes of the elements Ni, Co, Cr, Fe, and Mn as previously deduced from experiments on Ni, Ni-Co, Ni-Cr, and Ni-Fe binary alloys, and from Mn additions to various Co-Cr-Fe-Ni medium-entropy alloys [11]. To verify that the V atomic volume translates into a large misfit volume in Co-Cr-Fe-Mn-Ni-V alloys, we have also performed DFT calculations to compute the misfit volumes in random Ni_2V. In the DFT calculations, we compute the alloy atomic volumes of Ni-V alloys around the central composition, where c_{Ni} spans from 0.630 to 0.704. Then linear regression is performed to the DFT-computed alloy atomic volumes, which gives $V_{\text{alloy}} = 13.537 - 2.880c_{\text{Ni}}$ with $R^2 = 0.997$. This result then provides the DFT lattice constant of Ni_2V ($a = 3.595$ Å, $V_{\text{alloy}} = 11.617$ Å^3) and, more importantly, the misfit volumes $\Delta V_{\text{Ni}} = -0.960$ Å^3 and $\Delta V_{\text{V}} = 1.920$ Å^3. To remain consistent with the apparent volume of Ni (10.94 Å^3), the corresponding apparent volume of V is determined as 13.8 Å^3, in good agreement with the elemental fcc V volume. Therefore, when V is added to alloys in the Cantor alloy family, the large misfit of V is predicted to generate a high strengthening relative to all other alloying elements in this family, in spite of the fact that V leads to a small reduction in elastic modulus.

Applying the incorrect Voronoi method to Ni_2V would yield an apparent V volume of 11.8 Å^3. This value is very close to the literature DFT Voronoi volume for NiCoV [5], but is, unfortunately, significantly smaller than the accurate value 13.8 Å^3 derived here (Eq. 3). Other very recent literature [22] reports the apparent volume of V as 12.23 Å^3. However, this value was computed for V in Ni in the

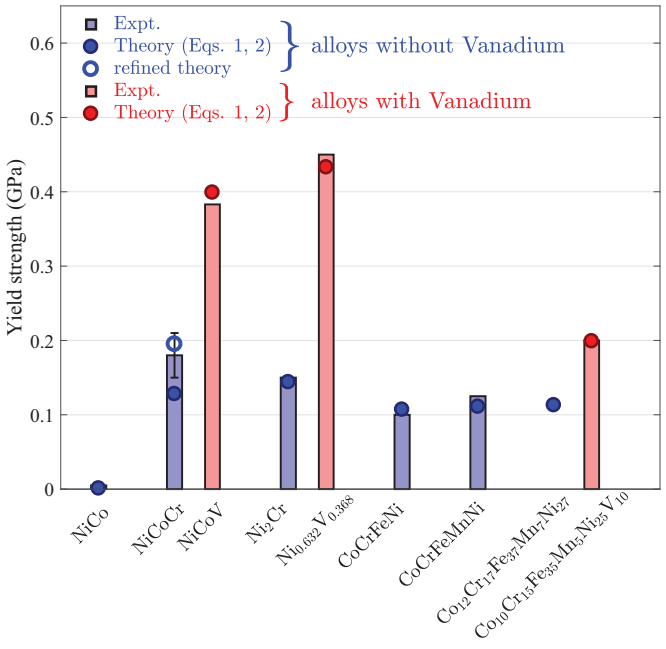

Fig. 1. Yield strength of various fcc HEAs with (red) and without (blue) Vanadium, at room temperature and loading rate of 10^{-3} s^{-1}, as measured (bars) and as predicted (symbols) by the isotropic theory (Eqs. (1) and (2)). The atomic volume of V as determined from Ni_2V is used in all V-containing alloys. The refined theory prediction of NiCoCr is based on anisotropic elasticity and the experimentally measured misfit volumes. (For interpretation of the references to colour in this figure legend, the reader is referred to the web version of this article.)

dilute limit (one V atom in a large cell). Our own calculations yielding 12.20 $Å^3$ confirm this dilute-limit value, but it differs significantly from the value at more appropriate concentrations, e.g., 13.8 $Å^3$ as computed here from Ni_2V.

Fig. 1 shows the experimental and predicted strengths of various alloys in the Co-Cr-Ni-V sub-family. Comparisons are made after subtracting the so-called Hall-Petch grain-size-dependent strengthening to reveal only the intrinsic "chemical" strength predicted by the theory. We use the analytic model of Eqs. (1) and (2) with Vegard's law, the atomic volumes in Table 1, and the experimental polycrystalline isotropic elastic constants. (See Appendix A for detailed materials parameters.) NiCo has near-zero misfit and near-zero strength relative to pure Ni. Literature results on binary Ni-Cr at large grain size [23] lead to an estimated strength for Ni_2Cr of $\sim$ 150 MPa while the theory predicts 144 MPa. NiCoCr has received considerable attention due to its high strength and exceptional fracture toughness among the Cantor alloy subsystems with equi-composition and fcc single-phase. The experimental values from recent single crystal data [24], multiplied by 3.06 for comparisons to polycrystal data, and various extrapolations from finite grain size polycrystalline data [18,25] are in the range 150–210 MPa. The predicted strength using Eqs. (1) and (2) is 128 MPa but an improved prediction using anisotropic elasticity for this fairly anisotropic alloy and the experimentally-measured misfit volumes in NiCoCr predicts 195 MPa [18].

Table 1
Apparent volumes of each element in fcc HEAs. The apparent volume of V is obtained from DFT calculations of fcc V and fcc Ni_2V. Other values were deduced from experiments on Ni, Ni-Co, Ni-Cr, and Ni-Fe binary alloys, and from Mn additions to various Co-Cr-Fe-Ni alloys.

	fcc apparent volumes V_n ($Å^3$)
V	13.914 (from DFT of fcc V) 13.8 (from DFT of Ni_2V, used in prediction)
Cr	12.27[a]
Mn	12.60[a]
Fe	12.09[a]
Co	11.12[a]
Ni	10.94[a]

[a] Ref. [11].

Overwhelmingly stronger are the NiCoV [5] and $Ni_{0.632}V_{0.368}$ [9] alloys recently been fabricated and tested. For NiCoV, we use the reported isotropic elastic constants $\mu = 72$ GPa, $\nu = 0.334$ and predict the yield stress at $T = 300$ K and $\dot{\epsilon} = 10^{-3}$ s^{-1} to be 399 MPa. This is in excellent agreement with the experimental value of 383 MPa obtained by extrapolating finite grain size data to infinite grain size. The theory then further indicates that the Ni-V binary alloys will be the strongest, because the binary uses only the smallest (Ni) and largest (V) elements. Because the prediction also depends on the dislocation Burgers vector $b = a/\sqrt{2}$ related to the alloy lattice constant a and the alloy elastic moduli, the optimal Ni-V binary alloy favors compositions below the equi-composition alloy. Using the theory of Eqs. (1) and (2), we predict the strength of $Ni_{0.632}V_{0.368}$ to be 433 MPa. The reported yield strength of $Ni_{0.632}V_{0.368}$ at grain size 8.1 μm is 750 MPa [9]. Using the Hall-Petch slope of NiCoV (864 MPa · $\mu m^{1/2}$) [5], the yield strength of $Ni_{0.632}V_{0.368}$ at infinite grain size is estimated as $\sim$ 450 MPa. This is again in good agreement with the theory. The theory predicts that no higher intrinsic yield strengths can be obtained across the entire family of Co-Cr-Fe-Mn-Ni-V alloys, and none have been reported to date.

To show the role of V more broadly, we examine another V-containing alloy recently fabricated and tested [26]. The alloy composition is $Co_{10}Cr_{15}Fe_{35}Mn_5Ni_{25}V_{10}$, which is near the widely-studied equi-composition CoCrFeNi and Cantor alloys but with a relatively small addition of V. The yield strength for this alloy at a very small grain size of 5.2 μm was measured to be 498 MPa. Extrapolating to infinite grain size using the average scaling for the closely-related CoCrFeNi (860 MPa · $\mu m^{1/2}$) [27] and Cantor alloy (494 MPa · $\mu m^{1/2}$) [28] leads to an intrinsic strength of $\sim$ 200 MPa. Application of the theory (Eq. 1 and 2) using the elastic moduli of the CoCrFeNi yields 199 MPa, as shown in Fig. 1. We predict that the same alloy without V, i.e., increasing all other components by 2 at.% for a composition $Co_{12}Cr_{17}Fe_{37}Mn_7Ni_{27}$ and with no change in elastic constants, would have a strength of only 113 MPa. By extrapolating to the infinite grain size, the experimental yield strength for the V-free CoCrFeNi and Cantor alloys are also only $\sim$ 100 MPa [27] and $\sim$ 125 MPa [28], respectively, with predicted strengths of 107 MPa and 111 MPa (see Fig. 1). Thus, again, V addition, even at a smaller (but non-dilute) concentration of 10 at.%, provides a large ($\sim$ 76%) increase in strengthening relative to the V-free counterparts, and the theory predicts this strengthening.

3.2. Application of theory to bcc HEAs

Turning to the bcc alloys, the atomic volumes of the bcc elements Cr, Mo, Nb, Ta, V, W have been measured experimentally [29], as shown in Table 2. Experimental studies of the lattice constants of various HEA alloys composed of these elements plus alloys containing Hf enable the estimation of Hf apparent volume based on Vegard's law [30]. For Ti and Zr, which exist in the bcc structure only at high temperatures, extrapolations are carried out to estimate the apparent volumes at room temperature [31,32]. Here, V stands out as the second-smallest element, with only Cr being smaller. However, Cr is smaller than V in both fcc and bcc and so although Cr can be potent for bcc alloys it is not nearly as effective as V in fcc alloys (see Fig. 1). Furthermore, fabrication of single-phase random bcc alloys containing Cr can be challenging due to the strong tendency of Cr to form embrittling intermetallic compounds. Only V is predicted to provide substantial strengthening in both fcc and bcc alloys.

The role of V in bcc alloys is first revealed through a comparison of the refractory alloys MoNbTaW and MoNbTaVW, which differ only by the addition of V replacing 5 at.% of each of the other 4 elements. The predictions of the theory and the experimental strengths versus

Table 2
Apparent volumes of elements in bcc HEAs. The apparent volumes of Ti and Zr are obtained by extrapolation of high temperature bcc data to room temperature, and that for Hf is from Vegard's law applied to experimental volumes of various Hf-containing HEAs. Other values are from the experimental lattice constants of the elements.

	bcc apparent volumes V_n (Å^3)
Cr	12.321[a]
V	14.020[a]
Mo	15.524[a]
W	15.807[a]
Ti	17.387[b] (high T extrapolated to RT)
Nb	17.952[a]
Ta	17.985[a]
Hf	22.528[c] (from Vegard's law on Hf-HEAs)
Zr	23.02[d] (high T extrapolated to RT)

[a] Ref. [29].
[b] Ref. [31].
[c] Ref. [30].
[d] Ref. [32].

temperature, as reported recently [12], are shown in Fig. 2. The V-containing alloy has a significantly higher strength over the entire temperature range. This is in spite of the fact that V has the lowest melting point of all of these elements, and elastic moduli that are ~ 10% lower than the 4-component alloy. The role of V is thus central to obtaining very high strength, as predicted. Many other bcc alloys in the Mo-Nb-Ta-V-W family also have high strengths, but there are no V-free counterparts in the literature; the theory predictions are consistent with these high strengths [12].

Examining other bcc alloy pairs where V is added, strengthening is found in all alloys. Fig. 2 summarizes results reported in Miracle-Senkov [3], Couzinié–Miracle–Senkov–Dirras [33], Senkov et al. [34], and Rao et al. [35]. In general, the predictions of the V-containing alloys are in good agreement (~15%) with the experiments. However, our predictions for the V-free alloys can be notably lower than experiments. One possible explanation is that there is a change from control of the alloy strength by edge dislocations (with V) to screw dislocations (without V) in some alloys. In addition, our predictions for MoNbTaTiW both without and with V are lower than experiments. This could be attributed to the possible presence of high (1–2 at.%) interstitial Oxygen and/or Nitrogen content, which was recently shown to increase strength by ~ 400 MPa at 2 at.% interstitial O or N (and usually causing embrittlement, see [36]). The presence of O and N could be particularly associated with the presence of Ti, consistent with experimental observations of increased strength upon Ti additions in some bcc alloys. Overall, in spite of some quantitative differences, all of the experimental evidence on bcc alloys points to the role of V in achieving high strength, as compared to other alloy additions. Within the Mo-Nb-Ta-V-W family, the theory further predicts that alloys $Ta_{0.33}V_{0.33+x}W_{0.33-x}$ with $-0.1 < x < 0.1$ will have the highest intrinsic strengths at high temperatures by taking advantage of both the large V misfit volume and the high stiffness of W. This prediction should drive experimental investigations of these alloys.

4. Conclusions

In summary, many new fcc and bcc high-entropy alloys have been fabricated with V as one of many elements, and these alloys have high strengths relative to their counterparts without V. However, the critical role of V has not been recognized or understood. The centrality of solute misfit volumes, over all other material properties, is revealed through recent theory for strengthening in these complex random alloys. The uniqueness of V then follows from its atomic volume in fcc and bcc crystals: larger in fcc and smaller in bcc than other HEA alloying elements, creating large misfit volume and high strengthening in both fcc and bcc alloys. This singular feature of V makes it the prime element for use as a strengthener in both fcc and bcc HEAs, both as measured and as predicted by theory. While strength is not the only application requirement, and the low-temperature formation of Vanadium oxide may limit applications of V-containing alloys in some situations, the general insight revealed here, along with the theoretical models, can drive experimental alloy design centered around V as a key elemental component.

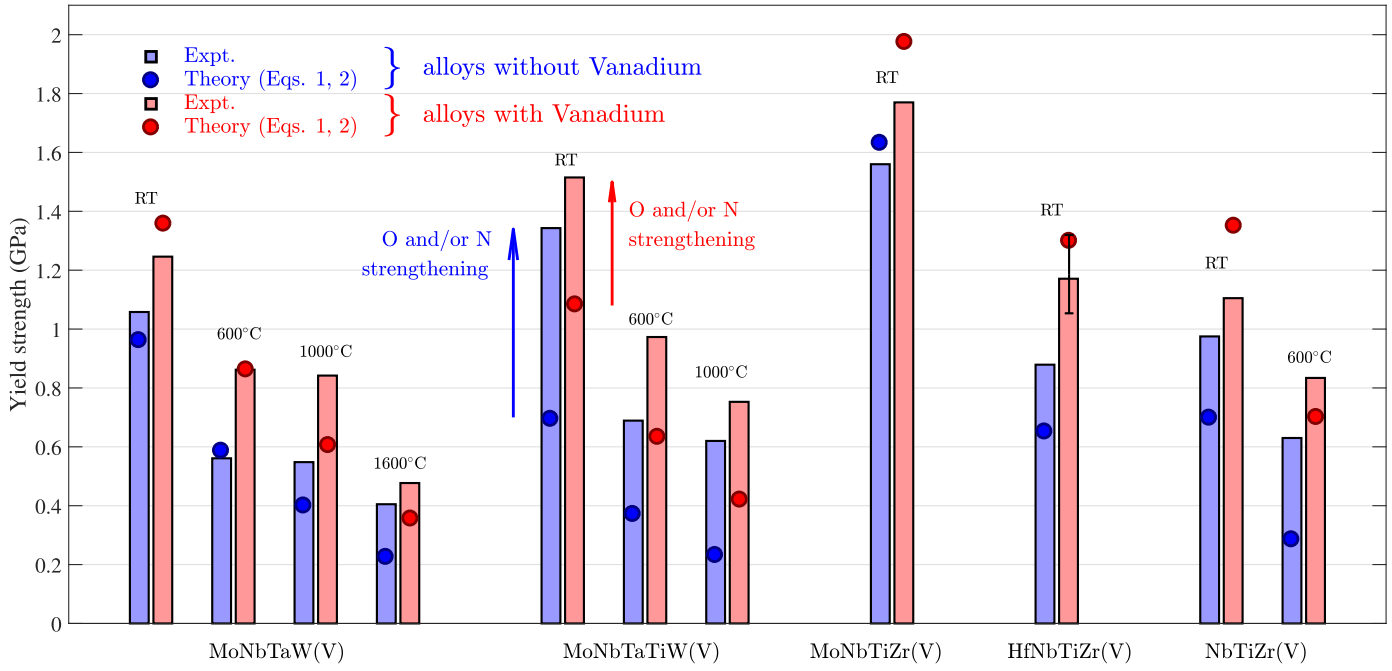

Fig. 2. Yield strength of various bcc HEAs with (red) and without (blue) Vanadium, at various temperatures and loading rate of 10^{-3} s^{-1} (loading rate 0.2×10^{-3} s^{-1} for MoNbTiZr(V)), as measured (bars) and as predicted (symbols). Some Ti-containing alloys could be strengthened by O and/or N impurities at concentrations of 1–2 at.%, as indicated. (For interpretation of the references to colour in this figure legend, the reader is referred to the web version of this article.)

Table 3
Material parameters used in the solute strengthening model and the predicted strength (at $T = 300$ K and $\dot{\epsilon} = 10^{-3}$ s^{-1}) for various fcc and bcc HEAs. The lattice constant and δ-parameter are computed using Vegard's law and the atom apparent volumes in Tables 1 and 2. Here, $\delta = \sqrt{\sum_n c_n \Delta V_n^2}/(3V_{\text{alloy}})$ describes the collective effect of misfit volumes, with $V_{\text{alloy}} = a^3/4$ for fcc and $V_{\text{alloy}} = a^3/2$ for bcc. Some elastic moduli are assumed to be the same as similar systems due to the lack of literature data.

	a (Å)	δ (%)	μ (GPa)	ν	σ_y (MPa) (Theory)	σ_y (MPa) (Exp RT)
NiCo	3.534	0.272	84[a]	0.26[a]	1	~ 5[a]
NiCoCr	3.577	1.716	87[a]	0.30[a]	128 195[c] (refined theory)	~ 150–210[d]
NiCoV	3.630	3.647	72[b]	0.334[b]	399	~ 383[b]
Ni_2Cr	3.571	1.836	87 (from NiCoCr)	0.30 (from NiCoCr)	144	~ 150[e]
$Ni_{0.632}V_{0.368}$	3.633	3.834	72 (from NiCoV)	0.334 (from NiCoV)	433	~ 450[f]
CoCrFeNi	3.594	1.672	84[a]	0.28[a]	107	~ 100[a]
CoCrFeMnNi	3.614	1.850	80[a]	0.26[a]	111	~ 125[a]
$Co_{12}Cr_{17}Fe_{37}Mn_7Ni_{27}$	3.607	1.714	84 (from CoCrFeNi)	0.28 (from CoCrFeNi)	113	-
$Co_{10}Cr_{15}Fe_{35}Mn_5Ni_{25}V_{10}$	3.627	2.353	84 (from CoCrFeNi)	0.28 (from CoCrFeNi)	199	~ 200[g]
MoNbTaW	3.228	2.291	103[h]	0.31[h]	954	~ 1058[i]
MoNbTaWV	3.192	3.124	92[h]	0.32[h]	1347	~ 1246[i]
MoNbTaTiW	3.235	2.084	87[h]	0.32[h]	688	~ 1343[i]
MoNbTaTiWV	3.204	2.945	81[h]	0.32[h]	1074	~ 1515[i]
MoNbTiZr	3.330	5.008	56[h]	0.35[h]	1661	~ 1560[i]
MoNbTiZrV	3.276	5.792	55[h]	0.35[h]	2008	~ 1770[i]
HfNbTiZr	3.432	4.227	29[h]	0.39[h]	643	~ 879[i]
HfNbTiZrV	3.361	5.932	34[h]	0.38[h]	1286	~ 1171[i]
NbTiZr	3.388	4.339	30[h]	0.39[h]	690	~ 975[j]
NbTiZrV	3.308	5.925	36[h]	0.38[h]	1337	~ 1105[i]

[a] Ref. [11].
[b] Ref. [5].
[c] Ref. [18].
[d] Refs. [18,25].
[e] Ref. [23].
[f] Ref. [9].
[g] Ref. [26].
[h] The anisotropic elastic constants C_{ij} of the alloy is estimated by applying "rule-of-mixtures" to the elemental C_{ij}, i.e., $C_{ij,\text{alloy}} = \sum_n c_n C_{ij,n}$. Then alloy isotropic elastic moduli are estimated (Bacon-Scattergood shear modulus $\mu = \sqrt{C_{44}(C_{11}-C_{12})/2}$, bulk modulus $B = (C_{11}+2C_{12})/3$, Poisson's ratio $\nu = \nu(\mu, B)$).
[i] Ref. [33].
[j] Ref. [34].

Declaration of interests

The authors declare that they have no known competing financial interests or personal relationships that could have appeared to influence the work reported in this paper.

Acknowledgments

This research was supported by the NCCR MARVEL, funded by the Swiss National Science Foundation. We also acknowledge support of high-performance computing provided by Scientific IT and Application Support (SCITAS) at EPFL.

Appendix A

For both fcc and bcc HEAs, the materials parameters that enter the solute strengthening model are summarized in Table 3. The resulting predictions are compared with the experimentally measured yield strength.

References

[1] E.P. George, D. Raabe, R.O. Ritchie, High-entropy alloys, Nat. Rev. Mater. 4 (2019) 515.
[2] Y. Ikeda, B. Grabowski, F. Körmann, Ab initio phase stabilities and mechanical properties of multicomponent alloys: a comprehensive review for high entropy alloys and compositionally complex alloys, Mater. Charact. 147 (2019) 464–511.
[3] D.B. Miracle, O.N. Senkov, A critical review of high entropy alloys and related concepts, Acta Mater. 122 (2017) 448–511.
[4] B. Gludovatz, A. Hohenwarter, D. Catoor, E.H. Chang, E.P. George, R.O. Ritchie, A fracture-resistant high-entropy alloy for cryogenic applications, Science 345 (2014) 1153–1158.
[5] S.S. Sohn, A. Kwiatkowski da Silva, Y. Ikeda, F. Körmann, W. Lu, W.S. Choi, B. Gault, D. Ponge, J. Neugebauer, D. Raabe, Ultrastrong medium-entropy single-phase alloys designed via severe lattice distortion, Adv. Mater. 31 (2019) 1807142.
[6] Z. Wang, Q. Fang, J. Li, B. Liu, Y. Liu, Effect of lattice distortion on solid solution strengthening of BCC high-entropy alloys, J. Mater. Sci. Technol. 34 (2018) 349–354.
[7] H. Song, F. Tian, Q.-M. Hu, L. Vitos, Y. Wang, J. Shen, N. Chen, Local lattice distortion in high-entropy alloys, Phys. Rev. Mater. 1 (2017) 023404.
[8] F. Körmann, M.H. Sluiter, Interplay between lattice distortions, vibrations and phase stability in NbMoTaW high entropy alloys, Entropy 18 (2016) 403.
[9] H.S. Oh, S.J. Kim, K. Odbadrakh, W.H. Ryu, K.N. Yoon, S. Mu, F. Körmann, Y. Ikeda, C.C. Tasan, D. Raabe, T. Egami, E.S. Park, Engineering atomic-level complexity in high-entropy and complex concentrated alloys, Nat. Commun. 10 (2019) 2090.
[10] Y.Y. Zhao, Z.F. Lei, Z.P. Lu, J.C. Huang, T.G. Nieh, A simplified model connecting lattice distortion with friction stress of Nb-based equiatomic high-entropy alloys, Mater. Res. Lett. 7 (2019) 340–346.
[11] C. Varvenne, A. Luque, W.A. Curtin, Theory of strengthening in FCC high entropy alloys, Acta Mater. 118 (2016) 164–176.
[12] F. Maresca, W.A. Curtin, Mechanistic origin of high strength in refractory BCC high entropy alloys up to 1900K, Acta Mater. 182 (2020) 235–249.
[13] C. Varvenne, W.A. Curtin, Predicting yield strengths of noble metal high entropy alloys, Scr. Mater. 142 (2018) 92–95.
[14] B. Yin, W.A. Curtin, First-principles-based prediction of yield strength in the RhIrPdPtNiCu high-entropy alloy, Npj Comput. Mater. 5 (2019) 14.
[15] O.N. Senkov, G.B. Wilks, J.M. Scott, D.B. Miracle, Mechanical properties of Nb25Mo25Ta25W25 and V20Nb20Mo20Ta20W20 refractory high entropy alloys, Intermetallics 19 (2011) 698–706.
[16] S. Gorsse, D.B. Miracle, O.N. Senkov, Mapping the world of complex concentrated alloys, Acta Mater. 135 (2017) 177–187.
[17] S. Nag, C. Varcenne, W.A. Curtin, Solute-strengthening in elastically anisotropic FCC alloys, Model. Simul. Mater. Sci. Eng. 28 (2020) 025007.
[18] B. Yin, S. Yoshida, N. Tsuji, W.A. Curtin, Yield strength and misfit volumes of NiCoCr and implications for short-range-order, Submitted (2020).
[19] G. Kresse, J. Furthmüller, Efficient iterative schemes for AB initio total-energy calculations using a plane-wave basis set, Phys. Rev. B 54 (1996) 11169–11186.
[20] J.P. Perdew, K. Burke, M. Ernzerhof, Generalized gradient approximation made simple, Phys. Rev. Lett. 77 (1996) 3865–3868.
[21] G. Kresse, D. Joubert, From ultrasoft pseudopotentials to the projector augmented-wave method, Phys. Rev. B 59 (1999) 1758–1775.
[22] D. Wen, C.-H. Chang, S. Matsunaga, G. Park, L. Ecker, S.K. Gill, M. Topsakal, M.A. Okuniewski, S. Antonov, D.R. Johnson, M.S. Titus, Structure and tensile

properties of Mx(MnFeCoNi)100-x solid solution strengthened high entropy alloys, Materialia 9 (2020) 100539.
[23] N. Clément, D. Caillard, J.L. Martin, Heterogeneous deformation of concentrated NiCr F.C.C. alloys: macroscopic and microscopic behaviour, Acta Metall. 32 (1984) 961–975.
[24] B. Uzer, S. Picak, J. Liu, T. Jozaghi, D. Canadinc, I. Karaman, Y.I. Chumlyakov, I. Kireeva, On the mechanical response and microstructure evolution of NiCoCr single crystalline medium entropy alloys, Mater. Res. Lett. 6 (2018) 442–449.
[25] M. Schneider, E.P. George, T.J. Manescau, T. Záležák, J. Hunfeld, A. Dlouhý, G. Eggeler, G. Laplanche, Analysis of strengthening due to grain boundaries and annealing twin boundaries in the CrCoNi medium-entropy alloy, Int. J. Plast. 124 (2020) 155–169.
[26] Y.H. Jo, S. Jung, W.M. Choi, S.S. Sohn, H.S. Kim, B.J. Lee, N.J. Kim, S. Lee, Cryogenic strength improvement by utilizing room-temperature deformation twinning in a partially recrystallized VCrMnFeCoNi high-entropy alloy, Nat. Commun. 8 (2017) 15719.
[27] Z. Wu, H. Bei, G.M. Pharr, E.P. George, Temperature dependence of the mechanical properties of equiatomic solid solution alloys with face-centered cubic crystal structures, Acta Mater. 81 (2014) 428–441.
[28] F. Otto, A. Dlouhý, C. Somsen, H. Bei, G. Eggeler, E.P. George, The influences of temperature and microstructure on the tensile properties of a CoCrFeMnNi high-entropy alloy, Acta Mater. 61 (2013) 5743–5755.
[29] G. Simmons, H. Wang, Single Crystal Elastic Constants and Calculated Aggregate Properties: A Handbook, The M.I.T. Press, 1971. https://mitpress.mit.edu/books/single-crystal-elastic-constants-and-calculated-aggregate-properties-second-edition.
[30] J.P. Couzinié, L. Lilensten, Y. Champion, G. Dirras, L. Perrière, I. Guillot, On the room temperature deformation mechanisms of a TiZrHfNbTa refractory high-entropy alloy, Mater. Sci. Eng. A 645 (2015) 255–263.
[31] W. Petry, A. Heiming, J. Trampenau, M. Alba, C. Herzig, H.R. Schober, G. Vogl, Phonon dispersion of the BCC phase of group-IV metals. I. BCC titanium, Phys. Rev. B 43 (1991) 10933.
[32] A. Heiming, W. Petry, J. Trampenau, M. Alba, C. Herzig, H.R. Schober, G. Vogl, Phonon dispersion of the BCC phase of group-IV metals. II. BCC zirconium, a model case of dynamical precursors of martensitic transitions, Phys. Rev. B 43 (1991) 10948.
[33] J.P. Couzinié, O.N. Senkov, D.B. Miracle, G. Dirras, Comprehensive data compilation on the mechanical properties of refractory high-entropy alloys, Data Br. 21 (2018) 1622–1641.
[34] O.N. Senkov, S. Rao, K.J. Chaput, C. Woodward, Compositional effect on microstructure and properties of NbTiZr-based complex concentrated alloys, Acta Mater. 151 (2018) 201–215.
[35] S.I. Rao, B. Akdim, E. Antillon, C. Woodward, T.A. Parthasarathy, O.N. Senkov, Modeling solution hardening in BCC refractory complex concentrated alloys: NbTiZr, Nb1.5TiZr0.5 and Nb0.5TiZr1.5, Acta Mater. 168 (2019) 222–236.
[36] Z. Lei, X. Liu, Y. Wu, H. Wang, S. Jiang, S. Wang, X. Hui, Y. Wu, B. Gault, P. Kontis, D. Raabe, L. Gu, Q. Zhang, H. Chen, H. Wang, J. Liu, K. An, Q. Zeng, T.G. Nieh, Z. Lu, Enhanced strength and ductility in a high-entropy alloy via ordered oxygen complexes, Nature 563 (2018) 546–550.